Molecular Pharmacology Fast Forward. Published on December 10, 2012 as doi: 10.1124/mol.112.081810
This article has not been copyedited and formatted. The final version may differ from this version.

Identification and characterization of a potent activator of p53-independent cellular senescence via a small molecule screen for modifiers of the Integrated Stress Response

Carly M. Sayers, Ioanna Papandreou, David M. Guttmann, Nancy L. Maas, J. Alan Diehl, Eric S. Witze, Albert C. Koong, and Constantinos Koumenis

Departments of Radiation Oncology (C.M.S, D.M.G., C.K.) and Cancer Biology (N.L.M., J.A.D., E.S.W.), Perelman School of Medicine, University of Pennsylvania, Philadelphia, Pennsylvania 19104.

Department of Radiation Oncology (I.P., A.C.K.), Stanford School of Medicine, Stanford, California 94305.

Molecular Pharmacology Fast Forward. Published on December 10, 2012 as DOI: 10.1124/mol.112.081810
This article has not been copyedited and formatted. The final version may differ from this version.

Running Title: Novel activator of cellular senescence

Corresponding Author: Constantinos Koumenis

Address: Department of Radiation Oncology, Univ. of Pennsylvania Perelman School of Medicine, Translational Research Center Room 8th Floor, 3400 Civic Center Blvd., Bldg 421, Philadelphia, PA 19104-5156

Tel.: (215) 898-0076

Fax: (215) 898-0090

Email: costas.koumenis@uphs.upenn.edu

Text pages: 35

Tables: 0

Figures: 7 (plus 2 supplementary and 2 videos)

References: 41

Words in Abstract: 250

Words in Introduction: 676

Words in Discussion: 1249

Abbreviations: ATF4, activating transcription factor 4; CDKI, cyclin-dependent kinase inhibitor; Chk2, checkpoint kinase 2; CHOP, DNA-damage-inducible transcript 3; CMV, cytomegalovirus; DCF-DA, 2′,7′-dichlorofluorescin diacetate; DMSO, dimethyl sulfoxide; eIF2α, eukaryotic translation initiation factor 2, subunit 1 alpha; ER, endoplasmic reticulum; ISR, integrated stress response; Luc, luciferase; MEF, mouse embryonic fibroblast; MG132, carbobenzoxy-Leu-Leu-leucinal; MTT, 3-(4,5-Dimethylthiazol-2-yl)-2,5-diphenyltetrazolium bromide; PARP, poly (ADP-ribose) polymerase 1; PBS, phosphate buffered saline; PI, propidium iodide; PERK, PKR-like endoplasmic reticulum kinase; ROS, reactive oxygen species; Tg, thapsigargin; UPR, unfolded protein response; UTR, untranslated region; XBP-1s, spliced X-box binding protein 1

Molecular Pharmacology Fast Forward. Published on December 10, 2012 as DOI: 10.1124/mol.112.081810
This article has not been copyedited and formatted. The final version may differ from this version.

Abstract

The Integrated Stress Response (ISR) is a signaling program which enables cellular adaptation to stressful conditions like hypoxia and nutrient deprivation in the tumor microenvironment. An important effector of the ISR is ATF4, a transcription factor that regulates genes involved in redox homeostasis and amino acid metabolism and transport. Because both inhibition and overactivation of the ISR can induce tumor cell death, modulators of ATF4 expression could prove to be clinically useful. In this study, chemical libraries were screened for modulators of ATF4 expression. We identified one compound, E235, which activated the ISR and dose-dependently increased levels of ATF4 in transformed cells. A dose-dependent decrease in viability was observed in several mouse and human tumor cell lines, and knockdown of ATF4 significantly increased the anti-proliferative effects of E235. Interestingly, low μM doses of E235 induced senescence in many cell types, including HT1080 human fibrosarcoma and B16F10 mouse melanoma cells. E235-mediated induction of senescence was not dependent on p21 or p53; however, p21 conferred protection against the growth inhibitory effects of E235. Treatment with E235 resulted in an increase in cells arrested at the G2/M phase with a concurrent decrease in S-phase cells. E235 also activated DNA damage response signaling, resulting in increased levels of Ser15-phosphorylated p53, γ-H2AX, and phosphorylated Chk2, although E235 does not appear to cause physical DNA damage. Induction of γ-H2AX was abrogated in ATF4 knockdown cells. Together, these results suggest that modulation of the ISR pathway with the small molecule E235 could be a promising anti-tumor strategy.

Introduction

The Integrated Stress Response (ISR) is a coordinated cellular program induced by cells to adapt to a multitude of stresses, including ER stress, hypoxia, low glucose, and amino acid deprivation (Kaufman, 2002; Lee, 1992). There are four known kinases that regulate the ISR: PERK (PKR-like endoplasmic reticulum kinase), GCN2 (general control non-derepressible 2), PKR (double stranded RNA activated protein kinase) and HRI (heme-regulated inhibitor kinase). PERK is a transmembrane ER protein that is activated by factors that induce ER stress, such as low glucose, hypoxia and unfolded proteins, whereas GCN2 is a cytoplasmic protein that is responsible for sensing low levels of amino acids (Shi et al, 1998; Wek et al, 1995). The others are HRI, which is activated by heme deficiency, and PKR, a kinase regulated by double stranded RNA (Chen, 2000; Levin et al, 1980). When any of these four kinases are activated, they can phosphorylate the translation initiation factor eIF2α (Blais et al, 2004; Koumenis et al, 2002). Phosphorylation of eIF2α results in general translation inhibition; however, a group of stress-response genes are translationally upregulated due to ribosome initiation at an alternate upstream open reading frame (Harding et al, 2000a; Shi et al, 1998; Vattem & Wek, 2004).

ATF4 is one of these genes, and it is of particular interest as it modulates the expression of genes involved in oxidative stress mitigation, amino acid synthesis, and uptake of nutrients (Blais et al, 2004; Harding et al, 2003; Vattem & Wek, 2004). It has been demonstrated by our group and others that the levels of ATF4 protein are increased in tumor cells as compared to normal tissue and that ablating the expression of this protein significantly decreases the mass of xenograft tumors in mice (Ameri et al, 2004; Bi et al, 2005; Ye et al, 2010). It has also been shown that ATF4 expression colocalizes with hypoxic regions in both murine and human tumors (Ameri et al, 2004; Bi et al, 2005). However, while phosphorylation of eIF2α and upregulation of ATF4 can enhance cell survival, hyperactivation of this signaling pathway can lead to permanent cell growth arrest or cytotoxicity due to cell prolonged inhibition of protein synthesis.

Molecular Pharmacology Fast Forward. Published on December 10, 2012 as DOI: 10.1124/mol.112.081810
This article has not been copyedited and formatted. The final version may differ from this version.

We have previously shown that upregulation of ISR signaling potentiates the cytotoxicity of the proteasome inhibitor bortezomib, a drug known to activate the unfolded protein response (UPR) (Fels et al, 2008; Obeng et al, 2006). In addition, extensive or prolonged activation of the ISR leads to the ATF4-dependent upregulation of CHOP, a pro-apoptotic protein (Friedman, 1996; Harding et al, 2000a). Cell growth arrest by overactivation of the ISR has been attributed to PERK- and eIF2α-dependent inhibition of cyclin D1, a key regulator of cell cycle progression (Brewer & Diehl, 2000).

Based on these observations that ATF4 plays an important role in cancer cell survival, we sought to identify compounds capable of modulating the expression of ATF4 (both inhibitors and activators). For this, we used a construct consisting of the 5' untranslated region (UTR) of the ATF4 mRNA fused to the luciferase gene. This reporter construct allowed us to use luciferase activity as a surrogate for ATF4 mRNA translation. Screening of over 160,000 small molecules from the Specs, Chembridge, ChemDiv and ChemRX chemical libraries resulted in the identification of a compound that caused the upregulation of ATF4 translation. Additional studies on this compound, E235, revealed potent anti-proliferative activity against many transformed cells. Interestingly, E235 failed to upregulate ATF4 activity in normal, untransformed human diploid fibroblasts. Further analysis revealed that E235 causes cellular senescence in a p53- and p21-independent manner, as well as a G2/M cell cycle arrest, also in a p21-independent manner. Knockdown of ATF4 did not substantially affect senescence, but it increased overall cytotoxicity induced by E235.

Our results demonstrate that E235 is a potent activator of cellular senescence in a p53- and p21-independent manner in various transformed cells. Moreover, our results have uncovered a novel link between cellular senescence and activation of the ISR and show that ATF4 induction can be used as a readout in small molecule screens for novel senescence inhibitors with anti-tumor potential.

Molecular Pharmacology Fast Forward. Published on December 10, 2012 as DOI: 10.1124/mol.112.081810
This article has not been copyedited and formatted. The final version may differ from this version.

Materials and Methods

Chemicals

E235 (E235-1756) was obtained from ChemDiv (San Diego, CA). The E235 chemical structure was drawn using KnowItAll® Informatics System from Bio-Rad (Hercules, CA). All cell culture reagents were from Gibco, except MEM (minimum essential medium), which was from Mediatech (Manassas, VA). Thapsigargin (Tg), puromycin, MG132, and nocodozole were purchased from Sigma-Aldrich (St. Louis, MO). Staurosporine was from MP Biomedicals (Solon, OH).

Cell culture and generation of stable cell lines

HT1080 human fibrosarcoma cells were obtained from ATCC (Manassas, VA), B16F10 mouse melanoma cells were a gift from Dr. Sandra Ryeom (University of Pennsylvania, Philadelphia, PA), p21-/- MEFs were a gift from Dr. Charles Scherr (St. Jude's Children's Hospital, Memphis, TN), p53-/- MEFs were a kind gift from the lab of Dr. Scott Lowe (Cold Spring Harbor Laboratory, Cold Spring Harbor, NY), and 4T1 mouse mammary carcinoma cells were a gift from Steve Albelda (University of Pennsylvania, Philadelphia, PA). These cells were cultured in Dulbecco's modified Eagle medium (DMEM). RPMI-8226 human multiple myeloma cells (ATCC) were grown in RPMI. Mouse adult lung fibroblasts (ALFs) were isolated in our lab from adult female mice (C57BL/6J, Jackson Laboratory, Bar Harbor, ME) and cultured in DMEM/F12. In all cases, the media was supplemented with penicillin, streptomycin, and 10% fetal bovine serum (FBS). AG1522 cells (Coriell Cell Repository, Camden, NJ) were grown in MEM supplemented with penicillin, streptomycin, 15% FBS, and non-essential amino acids (NEAA). HT1080 shATF4 cells were also supplemented with NEAA, as well as 55μM β-mercaptoethanol. To establish cells with stable knockdown of p21, B16F10 cells were transfected with pLKO or pLKO-shP21 plasmids (Sigma-Aldrich) using Lipofectamine2000 (Invitrogen, Grand Island, NY) and selected

Molecular Pharmacology Fast Forward. Published on December 10, 2012 as DOI: 10.1124/mol.112.081810
This article has not been copyedited and formatted. The final version may differ from this version.

with puromycin (2μg/ml and reduced to 0.5 μg/ml for maintenance). HT1080 empty lentiviral vector and shPERK cells were grown with 0.5μg/ml puromycin to maintain plasmid expression.

Chemical library screen

The ATF4-Luc fusion gene construct was used in the screen (see results section). 4000 cells/well were plated for 24 hrs in 384 well microplate format prior to induction of ER stress with Thapsigargin (250nM) for 16h and exposure to one compound per well (10-20μM).

Luciferase reporter assay

HT1080 cells expressing either a constitutively active CMV-driven luciferase plasmid (CMV-Luc) or a plasmid where the expression of the luciferase gene was driven by the 5'-UTR of the ATF4 mRNA (ATF4-Luc) were seeded in a 24-well plate, and then treated in duplicate the following day. After 4 or 8 hours of treatment, luciferase activity was quantified using the Luciferase Assay System from Promega (Madison, WI). Each well was read in triplicate in a white 96-plate. Luciferase activity in the ATF4-Luc cells was normalized to the activity in the corresponding CMV-Luc cells.

Immunoblot analysis

Immunoblotting was performed as previously described (Koumenis et al, 2002), with the exception that proteins were transferred to polyvinylidene fluoride membranes. Protein concentration was determined using Pierce® 660 nm Protein Assay Reagent (Thermo Scientific, Waltham, MA), in accordance to the manufacturer's instructions. Primary antibodies against the following proteins were used: ATF4, p53, p21 (Santa Cruz Biotechnology, Santa Cruz, CA), Ku80, eIF2α, p-eIF2α, PERK, p-p53 (Ser15), cleaved caspase-3, p27, ubiquitin, p-Chk2 (Thr68), cleaved PARP (Cell Signaling Technology, Danvers, MA), β-actin (Sigma-Aldrich), γ-H2AX (Upstate Biotechnology, Inc., Lake Placid, NY) and p21 (BD Pharmingen, San

Molecular Pharmacology Fast Forward. Published on December 10, 2012 as DOI: 10.1124/mol.112.081810
This article has not been copyedited and formatted. The final version may differ from this version.

Diego, CA). Horseradish peroxidase-conjugated anti-mouse or anti-rabbit secondary antibodies (Thermo Scientific) were used to detect the primary antibodies, and then the immunoreactive bands were visualized on x-ray film (Thermo Scientific) using Amersham^{TM}ECL^{TM} or ECL Plus Western Blotting Detection Systems (GE Healthcare, Fairfield, CT). Pixel intensity of individual bands was quantified using ImageJ software (National Institutes of Health, Bethesda, MD).

Real-time quantitative PCR

RNA was isolated by using TRIzol® Reagent (ambion, Carlsbad, CA) and following the protocol provided with it. Reverse transcription was performed using AMV Reverse Transcriptase (Promega). Real-time quantitative PCR was done using Power SYBR® Green PCR Master Mix (Applied Biosystems, Carlsbad, CA) and was analyzed with the Applied Biosystems 7300 Real-Time PCR System. PCR primers were purchased from Invitrogen. The following primers were used: human XBP1s-F: 5'-CCGCAGCAGGTGCAGG, and XBP1s-R: 5'-GAGTCAATACCGCCAGAATCCA; human 18s rRNA-F: 5'-CAATTACAGGGCCTCGAAAG, and 18s rRNA-R: 5'-AAACGGCTACCACATCCAAG.

Cell viability assay

Cell viability was analyzed using the Cell Proliferation Kit I (MTT assay) (Roche Diagnostics, Indianapolis, IN) according to the manufacturer's protocol. Briefly, cells were seeded at low density in 24-well plates, and then treated in duplicate the following day. Once the DMSO-treated cells reached confluence, the MTT assay was started. To assess the effect of treatment length on cell viability, cells were plated at low density and treated for various lengths of time. The media with E235 was then removed and replaced with normal media and cells were allowed to proliferate until the untreated cells reached confluency (5 days after initial treatment). Each well was read in triplicate in a 96-well plate at absorbances of 550 and 690nm.

Molecular Pharmacology Fast Forward. Published on December 10, 2012 as DOI: 10.1124/mol.112.081810
This article has not been copyedited and formatted. The final version may differ from this version.

Live cell imaging

Cells were seeded at low density on 8-well chambered cover glass slides. Cells were viewed with a Leica AF6000 microscope (Wetzlar, Germany) at 37°C with 5% CO_2, and still images were captured every 20 minutes for 50 hours. Images were viewed and analyzed with Leica Application Suite AF.

SA-β-galactosidase staining

Staining for senescence-associated β-galactosidase (SA-β-gal) activity was performed using the Senescence β-Galactosidase Staining kit (Cell Signaling Technology) according to the instructions provided by the manufacturer. Brightfield images were captured on a Nikon Eclipse TE2000-U (Tokyo, Japan) using Image-Pro Plus 6.0 software (MediaCybernetics, Rockville, MD).

Clonogenic survival assay

Cells were plated at high density and allowed to attach overnight. They were then treated with E235 for 24 hours, at which time the cells were trypsinized and reseeded at low density in media without E235. The cells were incubated at 37°C for several days until colonies were of sufficient size to count. The colonies were fixed with 10% methanol/10% acetic acid and then stained with 0.4% crystal violet. Colonies were scanned and counted with an Oxford OptronixGelCount™ and its accompanying software (Oxford, UK).

Cell cycle analysis

Cells were treated with DMSO or E235 for 8h, 16h, or 24h and then harvested with trypsin. Harvested cells were washed, resuspended in PBS with 1%FBS, and fixed with cold ethanol. Fixed cells were washed, incubated in phosphate-citric acid buffer for 5 minutes and then resuspended in PI/RNase solution (PBS, RNase, and 50μg/ml propidium iodide) for staining.

Molecular Pharmacology Fast Forward. Published on December 10, 2012 as DOI: 10.1124/mol.112.081810
This article has not been copyedited and formatted. The final version may differ from this version.

The cells were incubated in this solution for 15 minutes at 37°C in the dark and then analyzed by flow cytometry with a BD FACSCalibur (BD Biosciences, San Jose, CA) and with FlowJo software (Tree Star, Inc., Ashland, OR).

ROS assay

B16F10 cells were treated with DMSO or various doses of E235 for 4h or with 50μM H_2O_2 for 2h. Cells were trypsinized, resuspended in PBS containing 10μM 2′,7′-dichlorofluorescin diacetate (DCF-DA) (Sigma-Aldrich), and incubated at 37°C for 30min. The cells were then spun down, resuspended in PBS, and analyzed by flow cytometry with a BD FACSCalibur (BD Biosciences) and with FlowJo software (Tree Star, Inc.).

Comet assay

DNA damage was investigated by the alkaline comet assay using the Trevigen Comet Assay™ kit (Trevigen Inc., Gaithersburg, MD). Briefly, cells were trypsinized and resuspended in cold PBS at 1×10^5 cells/ml. An aliquot of this single cell suspension was diluted 1:10 in LM Agarose. 50 μl of this suspension was added immediately to a CometSlide™ which was incubated at 4°C in the dark for 15 minutes and then immersed in pre-chilled lysis solution at 4°C for 30 min. The DNA was denatured in an alkaline solution (300 mM NaOH, 1 mM EDTA, pH>13) for 60 min at room temperature. Slides were subjected to electrophoresis under alkaline conditions (30 mM NaOH, 2 mM EDTA), at 4°C in the dark at 0.6 V/cm with a current of 35-40 mA for 25 minutes, rinsed twice in H_2O, and once in 70% EtOH, for five minutes each at room temperature. Slides were dried at 42°C and stained with SYBR green for 5 minutes at 4°C in the dark. DNA comets were visualized on an Olympus IX51 fluorescence microscope. Median tail moment was recorded from 100 comets per sample and quantified using Comet Assay IV software (Perceptive Instruments, UK).

Molecular Pharmacology Fast Forward. Published on December 10, 2012 as DOI: 10.1124/mol.112.081810
This article has not been copyedited and formatted. The final version may differ from this version.

Results

Identification of E235 as a modulator of ATF4 response. The ATF4 gene product is a crucial mediator of the response to both ER stress and nutrient deprivation in cells. It has been demonstrated that fusion of the ATF4 5'-UTR to luciferase (Fig. 1A) confers substantial upregulation of luciferase expression when cells are exposed to pharmacological activators of the UPR (e.g., Thapsigargin or tunicamycin) (Vattem & Wek, 2004). For screening of small molecule libraries, we used HT1080 cells stably expressing the ATF4 5'UTR-luciferase construct for the primary screens. The chemical library at Stanford University represents an expanded diverse small molecule library with compounds obtained from Specs, Chembridge, and ChemRX and Chemdiv. Compounds with Z factor scores of >0.5 were further evaluated in an expanded secondary screen, utilizing HT1080 cells expressing CMV-luciferase, XBP1-luciferase, and ATF4 5'UTR-luciferase. In the secondary screen, we assessed the ATF4-Luc modifying activity of each screening hit over a concentration range of up to 3 logs. Compounds that specifically blocked or activated ATF4 levels without significantly affecting control CMV-luc levels were further tested. Four compounds exhibiting these properties with an IC_{50} < 10 μM were identified. Of these, three compounds turned out to be false-positives, as they failed to significantly modify ATF4-Luc activity in triplicate experiments (not shown). One compound, E235, was a potent activator of ATF4. Since pharmacological activators of the UPR (e.g., Bortezomib, thapsigargin, etc) can have potent antiproliferative and antitumor effects, we decided to further investigate the *in vitro* properties of E235 against a variety of normal and transformed cells.

E235 Increases ATF4 Expression in Transformed Cells. Since E235 was identified in a chemical library screening for modulators of ATF4 expression, we first assessed the effect of

Molecular Pharmacology Fast Forward. Published on December 10, 2012 as DOI: 10.1124/mol.112.081810
This article has not been copyedited and formatted. The final version may differ from this version.

this drug on ATF4 protein expression (Fig.1B). E235 caused a dose-dependent increase in luciferase activity from a reporter plasmid containing the 5' UTR of the ATF4 mRNA fused to the luciferase gene (Fig. 1A,C). To confirm that this increase in luciferase activity corresponded to an increase in ATF4 protein levels, nuclear extracts from HT1080, B16F10, and AG1522 cells treated with increasing doses of E235 were subjected to immunoblotting. A dose-dependent increase in ATF4 protein levels was seen only in the HT1080 and B16F10 cells (Fig. 1D,E). There was no appreciable induction of ATF4 protein in the normal diploid AG1522 human fibroblasts in response to E235, whereas thapsigargin induced a potent upregulation of ATF4 levels (Fig. 1F), suggesting that this effect is restricted to transformed cells.

E235 Activates the ISR in Transformed Cells. Next, we analyzed the effects of E235 on the induction of the UPR and the ISR, since ATF4 is a common downstream effector of these two pathways. An intermediate dose of 1μM E235 was added to HT1080 cells for various lengths of time. HT1080 cells were also treated with increasing doses of E235 for 4h. There was a time- and dose-dependent induction of p-eIF2α in response to E235 (Fig. 2A,B). However, in contrast to thapsigargin, E235 failed to induce any significant change in the electrophoretic mobility of PERK. In agreement with the ATF4 results, this dose-dependent increase in p-eIF2α was not seen in the AG1522 cells (Fig. 2C). To determine if E235-mediated phosphorylation of eIF2α was a consequence of the activation of the UPR, the levels of spliced XBP-1 (XBP-1s) mRNA in HT1080 cells treated with E235 were evaluated by quantitative PCR. A very modest increase in XBP-1s was seen at 4h, but this was much less than the levels induced by thapsigargin, which suggested that E235 is acting primarily through the ISR (Fig. 2D). To determine if the E235-induced phosphorylation of eIF2α was PERK-dependent, immunoblotting for total PERK and p-eIF2α in both empty lentiviral vector- and shPERK-transduced HT1080 cells was performed. An increase in p-eIF2α was observed with 2h of E235 treatment in both the empty vector cells and the shPERK cells, suggesting that activation of the ISR by E235 was PERK-independent (Fig.

Molecular Pharmacology Fast Forward. Published on December 10, 2012 as DOI: 10.1124/mol.112.081810
This article has not been copyedited and formatted. The final version may differ from this version.

2E). Moreover, we tested whether the activation of the ISR was due to inhibition of the proteasome by treating HT1080 cells with various doses of E235 and comparing the levels of ubiquitinated proteins to those in cells treated with the known proteasome inhibitor MG132 (Fig. S1A). Minimal accumulation of ubiquitinated proteins was seen with even the highest concentration of E235, indicating that proteasomal activity was not being inhibited at doses which induce ATF4 expression.

E235 Inhibits Cell Proliferation. Previously, it was shown that while induction of ATF4 is generally cytoprotective, prolonged or excessive activation of the UPR and ISR can be cytotoxic (Fels et al, 2008; Zinszner et al, 1998). Thus, several transformed cell lines were treated with E235 and then subjected to an MTT viability assay. All four of the cancer cell lines tested exhibited a significant decrease in survival when treated with low μM concentrations of E235. E235 caused a dose-dependent decrease in cell viability in the HT1080 cells (Fig. 3A). Treatment with 1μM E235 decreased cell viability by over 75% in the B16F10 and 4T1 cells (Fig. 3A). A dose of 10μM E235 essentially blocked the growth of all four cell types. Trypan blue exclusion assays performed under similar conditions on HT1080 and B16F10 cells confirmed that E235 dose-dependently decreases cell viability (data not shown). Notably, doses as low as 0.25μM were sufficient to eliminate cell survival in the RPMI-8226 cells (Fig. 3A). In a clonogenic survival assay, 24h of 1μM E235 treatment completely prevented the formation of any colonies (Fig. S1B). In addition, HT1080 cells demonstrated a time-dependent decrease in cell viability, with 24h of E235 treatment reducing viability by more than 50% (Fig. 3B). Treatment of RPMI-8226 cells with E235 for just 8h was enough to abolish any cell survival (Fig. 3B). A dose dependent reduction in cell proliferation was also seen in the normal AG1522 cells, with 1μM E235 causing a 60-70% decrease in viability (Fig. 3C). To determine whether the observed decrease in cell viability was due to apoptosis, HT1080 and B16F10 cells were treated with E235 for various times and doses and the cleavage of PARP (c-PARP) and the processing

Molecular Pharmacology Fast Forward. Published on December 10, 2012 as DOI: 10.1124/mol.112.081810
This article has not been copyedited and formatted. The final version may differ from this version.

of caspase3 were examined by immunoblotting. While there was a modest increase in the 19kDa cleavage product of caspase3 in the HT1080 cells with E235, there was no significant accumulation of the 17kDa subunit, which was observed in the staurosporine-treated HT1080 cells (Fig. 3D). In the B16F10 cells treated with E235 for 24h, there was a small increase in caspase3 cleavage with increasing dose (Fig. 3E). In both cell lines, the levels of cleaved PARP in E235-treated samples remained the same as those in untreated controls. Together, these results suggest that apoptosis has a minimal contribution to the decrease in cell viability and proliferation induced by E235.

ATF4 Dependence of E235-Induced Effects. Because we have shown that treatment with E235 increases ATF4 expression, we sought to determine if cell viability during E235 treatment was dependent on ATF4 expression. An MTT assay was performed on E235-treated HT1080 cells stably transfected with either non-targeting shRNA (shNT) or shRNA directed at ATF4 (shATF4) (Fig. 4A). We observed a substantial decrease in cell viability in shATF4 cells compared to shNT cells at E235 doses of 0.5 and 1μM (Fig. 4B). In agreement with these results, a significant decrease in shATF4 cell viability compared to shNT cells was seen with low doses of E235 treatment in a clonogenic survival assay (Fig. 4C). However, 10μM doses of E235 eliminated cell survival in both shNT and shATF4 cells. Altogether, these results indicate that the induction of ATF4 confers cytoprotection to cells treated with low μM doses of E235.

E235 is a Potent Inducer of Cellular Senescence. While assaying the antiproliferative effects of E235 on transformed cells, we observed that cells treated for at least 48h with lower doses of E235 (0.25-1μM) increased in size and displayed characteristics consistent with a senescent phenotype (Fig. 5A). A small augmentation of cell size was also seen in normal mouse and human cells, but it was not as extensive as that observed in the transformed cells (Fig. 5A, S1C). We therefore assayed for SA-β-gal activity, a commonly used senescence marker. Both

HT1080 and B16F10 cells exhibited a dramatic increase in perinuclear SA-β-gal staining after 48h of treatment with lower doses of E235, with almost all of the cells treated with 1μM E235 being positive for β-gal expression (Fig. S1C and data not shown). In addition, these E235-induced morphological changes appeared to be irreversible, as cells retained their senescence-like appearance even 10 days after removal of the drug (data not shown). To determine the kinetics of the morphological changes, HT1080 and B16F10 cells were imaged via live microscopy (supplemental video files 1 and 2). We observed that the increase in cell size with 1μM E235 commenced approximately 24h post-treatment. We also noted a substantial reduction in cell proliferation in the E235-treated cells, which was consistent with the results from the MTT assays and supported our hypothesis that E235 was causing cells to undergo senescence.

To further examine the possibility that E235 induced senescence, levels of the cyclin-dependent kinase inhibitors (CDKI) p16, p21, and p27 with and without E235 treatment were assessed at various time points. Increased expression of these CDKIs has been correlated to the induction of cellular senescence (Ewald et al, 2010). Both HT1080 and B16F10 cells displayed elevated levels of p21 with 1μM E235 at 8 and 16h (Fig. 5B,C). In addition, a dose-dependent increase in p21 protein expression was seen with 24h of E235 treatment in the HT1080 cells (Fig. 5B). However, there was no appreciable difference in p27 levels in either cell type at any time point or any dose of E235 (Fig. 5B,C). We also did not observe any changes in p16 expression at either 24 or 48h after E235 treatment in the HT1080 cells (Fig. S1D).

E235-Induced Senescence is not Dependent on p21 or p53. Since E235 was shown to induce p21 protein expression, we wanted to investigate the role of p21 in E235-induced cellular senescence. B16F10 cells were transfected with a plasmid expressing shRNA directed at p21 (shP21) or with an empty vector plasmid (pLKO), and near complete knockdown of p21 was confirmed by Western blotting (Fig. S2A). These cells were then stained for SA-β-gal activity

after 48h of treatment with low doses of E235. Unexpectedly, shP21 cells were still able to assume senescence-like morphology and to exhibit staining for SA-β-gal activity (Fig. 5D). However, the p21 knockdown cells still showed a small induction of p21 protein expression after E235 treatment, which could have been sufficient for senescence to occur (Fig. S2A). To further test the role of p21, we treated p21+/+ and p21-/- MEFs with E235. We observed no difference in the ability of p21-/- vs. p21+/+ MEFs to undergo senescence (Fig. S2B). Nevertheless, there was a significant reduction in cell viability in two separate clones of shP21 cells treated with E235 (0.5 or 1μM) compared to pLKO-transfected controls (Fig. 5E). These results indicate that p21 plays a role in cellular survival but not senescence in E235-treated cells.

Because p53 is frequently involved in, although not absolutely required for, induction of cellular senescence (Ben-Porath & Weinberg, 2005; Chang et al, 1999), we tested the effects of E235 on p53 wild-type and knockout Ras- and myc-transformed MEFs. Interestingly, p53 was also found to be dispensable for E235-induced senescence, as p53 knockout cells retained their ability to senesce under low doses of E235 (Fig. S2C).

E235 Induces a G2/M Arrest. Consistent with the induction of senescence, we also observed that low doses of E235 caused cells to undergo G2/M arrest. The percentage of HT1080 cells in the G2/M phase of the cell cycle was significantly increased by E235 treatment, starting as early as 8h and becoming more evident at 16 and 24h (Fig. 6A). This E235-induced increase of cells in G2/M was accompanied by a concomitant reduction of cells in S phase, with only 14.5% of E235-treated cells in S phase at 24h compared to 38.8% of DMSO-treated cells (Fig. 6A). A small rise in the amount of cells in G1 was also observed. In addition, a substantial increase of cells in G2/M and concurrent decrease in S phase cells was seen even at 8h when B16F10 cells were treated with E235 (Fig. 6B).

Molecular Pharmacology Fast Forward. Published on December 10, 2012 as DOI: 10.1124/mol.112.081810
This article has not been copyedited and formatted. The final version may differ from this version.

Effects of E235 on DNA Damage Signaling Pathways and DNA Integrity. Since the majority of chemotherapeutic agents that cause cellular senescence have been shown to induce DNA damage, we next examined the effects of E235 on stabilization and phosphorylation of p53, a key regulator of the DNA damage response (Levine, 1997). Increasing doses of E235 corresponded to an increase in p53 protein levels in both normal (AG1522) and transformed (HT1080) cells (Fig. 7A). We also analyzed the phosphorylation of p53 at Ser15, which is associated with activation of the DNA damage response (Chao et al, 2000). In AG1522 cells, 1μM E235 induced a small amount of Ser15 phosphorylation, while 5 and 10μM doses produced p-Ser15 levels comparable to those seen in cells treated with 4Gy (Fig. 7B). We also observed a dose-dependent increase in p-Ser15 levels in E235-treated HT1080 cells (Fig. 7B). Levels of p-Chk2 and γ-H2AX were then examined to see if treatment with E235 also led to activation of the DNA damage response. In HT1080 cells, there was a significant induction in phosphorylation of H2AX with increasing doses of E235 (Fig.7C). This effect was significantly attenuated in AG1522 cells, where a concentration of at least 5μM E235 was required to see any γ-H2AX (Fig. 7C). Interestingly, the induction of γ-H2AX by E235 was attenuated in HT1080 cells expressing shATF4, suggesting that the DNA damage signaling could be partially dependent on ATF4 expression (Fig. 7E). E235 treatment caused an increase in the levels of phosphorylated Chk2 in both synchronized (with nocodazole) and unsynchronized HT1080 cells (Fig. 7D). The induction of the DNA damage response was not due to the generation of reactive oxygen species (ROS), however, even in cells treated with doses of up to 10μM E235 (Fig. S2D). To determine whether the activation of DNA damage response signaling was due to physical DNA damage, a comet assay was performed on AG1522 and HT1080 cells. E235 did not lead to DNA strand breaks in the AG1522 cells, as evidenced by the similar tail moments between the DMSO-treated and E235-treated cells (Fig. 7G). Even more surprising was the finding that E235 did not cause an increase in tail moment in the HT1080 cells, despite the high

Molecular Pharmacology Fast Forward. Published on December 10, 2012 as DOI: 10.1124/mol.112.081810
This article has not been copyedited and formatted. The final version may differ from this version.

levels of p53, Chk2 and H2AX phosphorylation (Fig. 7F,G). Therefore, E235 appears to elicit a DNA damage response without inducing physical DNA damage.

Molecular Pharmacology Fast Forward. Published on December 10, 2012 as DOI: 10.1124/mol.112.081810
This article has not been copyedited and formatted. The final version may differ from this version.

Discussion

It has been previously demonstrated that inhibition of the ISR pathway, whether by inhibiting PERK activity, eIF2α phosphorylation, or ATF4 expression, sensitizes cells to ER stress (Harding et al, 2000b; Scheuner et al, 2001; Ye et al, 2010). This sensitization is due to the accumulation of unfolded proteins in the ER and results in an increase in the levels of apoptosis (Koumenis, 2006). However, a key aspect of the ISR is that under certain biological contexts (e.g., hyperactivation by pharmacological agents, prolonged activation, etc.), it can also lead to cytotoxicity. With sustained activation of the ISR, cells can undergo permanent cell growth arrest by PERK-dependent inhibition of cyclin D1 (Brewer & Diehl, 2000). Alternatively, overactivation of the ISR can lead to cell death due to inhibition of protein synthesis and/or ATF4-mediated induction of the pro-apoptotic protein CHOP (Friedman, 1996; Harding et al, 2000a; Harding et al, 2000b). Our group has previously shown that have shown that hypoxia, a physciological activator of ER stress, increases the sensitivity of HeLa cells to the ER-stress inducing agents thapsigargin and bortezomib (Fels et al, 2008).

In this manuscript, we describe the identification of a novel, potent activator of cellular senescence, E235. The ISR and the UPR are increasingly being recognized as attractive targets for antitumor agents. Our screen was not able to identify any effective inhibitors of the PERK-eIF2α-ATF4 arm of the ISR. This may have been because the number of compounds screened was moderate (65,000), compared to larger, more encompassing chemical libraries. It is possible that screening of additional libraries may reveal specific inhibitors of this pathway. No specific inhibitors of this pathway have yet been reported in the literature.

We did, however, identify a potent activator of ATF4 expression with our screening assay. This compound, E235, was active at high nM to low μM concentrations in inducing upregulation of

Molecular Pharmacology Fast Forward. Published on December 10, 2012 as DOI: 10.1124/mol.112.081810
This article has not been copyedited and formatted. The final version may differ from this version.

ATF4-Luc activity and ATF4 protein expression in a variety of human and mouse transformed cells. Intriguingly, E235 was unable to induce robust upregulation of eIF2α phosphorylation or ATF4 expression in untransformed human diploid fibroblasts. This finding suggests that the mechanism of ISR activation by E235 is tumor cell-specific. Moreover, E235 displayed potent anti-proliferative activity against transformed cell lines without causing significant apoptosis. Rather, careful analysis of the effects of E235 using time-lapse microscopy revealed that it induced cellular senescence. This effect extended to the normal human fibroblasts. However, since normal tissues are not rapidly proliferating *in vivo*, and given the lack of any direct cytotoxicity by E235, we believe that *in vivo* this agent should display low toxicity towards normal tissues.

One caveat that must be considered is the fact that senescent cells can both suppress and promote tumor formation (Rodier & Campisi, 2011). Traditionally, senescence is considered to be anti-tumorigenic, as it suppresses two of the major hallmarks of cancer cells: expanded growth potential and the ability to continue proliferation in the presence of activated oncogenes (Hanahan & Weinberg, 2000). The results of several studies support this, demonstrating that senescent cells are commonly present in premalignant lesions but decrease in frequency in malignant tumors (Bartkova et al, 2005; Braig et al, 2005; Chen et al, 2005; Collado et al, 2005; Michaloglou et al, 2005). On the other hand, senescent cells have been shown to secrete many factors that promote tumor progression, such as interleukin-6 and -8 and matrix metalloproteases, which can stimulate basement membrane invasion, and vascular endothelial growth factor A and growth-related oncogene α, angiogenesis-inducing factors (Coppé et al, 2006; Coppé et al, 2010; Coppé et al, 2008; Kang et al, 2003; Ksiazek et al, 2008; Millis et al, 1992). These findings are reinforced by the fact that co-injection of premalignant epithelial cells that are not normally tumorigenic with senescent fibroblasts promotes cancer formation *in vivo*

Molecular Pharmacology Fast Forward. Published on December 10, 2012 as DOI: 10.1124/mol.112.081810
This article has not been copyedited and formatted. The final version may differ from this version.

(Krtolica et al, 2001). Therefore, studies will need to be performed to ensure that E235 does not promote the progression of premalignant lesions *in vivo*.

Mechanistically, E235 primarily induced a cell cycle arrest at the G2/M checkpoint. This was accompanied by potent activation of DNA damage signaling, as evidenced by increased phospho-p53 (ser15), Chk2, and γ-H2AX in transformed cells. Notably, DNA damage signaling was significantly attenuated in normal human fibroblasts, with marginal induction of these markers. Moreover, this activation of the G2/M checkpoint and DNA damage signaling was not accompanied by any significant increase in physical DNA damage, since we failed to observe any increase in DNA tail moment by the sensitive COMET assay. In contrast, a single dose of 4Gy elicited a substantial increase in tail moment in the same cells. Collectively, our results indicate that E235 causes cellular senescence by inducing DNA damage signaling in actively dividing transformed cells but not in normal fibroblasts. Although we also observed a strong induction of the CDKI, p21, by E235, this increase was not necessary for the induction of senescence, since E235 induced similar levels of senescence in p21-deficient and p21-proficient MEFs. However, B16F10 cells with knocked down p21 expression exhibited lower overall viability, indicating that p21-mediated cell cycle arrest must play a small, but significant, cytoprotective role.

Despite a robust upregulation of ATF4 translation by E235, the induction of senescence was not dependent on ATF4, as both HT1080 shATF4 cells and ATF4 -/- MEFs senesced when treated with low doses of E235 (data not shown). In addition, decreased expression of ATF4 did not significantly alter the cell cycle distribution of cells treated with 1μM E235 (data not shown). However, abrogation of ATF4 expression did lead to decreased levels of DNA damage signaling (γ-H2AX). This might provide a potential explanation for the increased sensitivity of shATF4 cells to E235, as the induction of DNA damage signaling could allow cells to ameliorate

the stress induced by E235. Also, as we have shown that shP21 cells are more sensitive to E235, p21 upregulation by DNA damage signaling may contribute to the cytoprotective role of ATF4. Hence, the increase in clonogenic cell death in ATF4 knockdown cells could be attributed to a decrease in DNA damage signaling, resulting in reduced p21 induction (Fig. S2E). Additional studies will be essential to confirm this and to further elucidate the effects of E235-mediated ATF4 induction on overall survival.

Although we have eliminated several potential mechanisms for induction of senescence by E235, such as induction of p21 or ATF4, inhibition of Aurora A (not shown), and induction of ROS, we still do not know exactly how E235 elicits its pro-senescence effects. It is possible that it may affect the process of DNA replication without inducing DNA damage or it could be a histone deacetylase inhibitor. A panel of over 400 known kinases was screened to determine if E235 exhibited inhibitory activity against any specific kinases (KINOMEscan, a division of DiscoveRx, San Diego, CA) (results not shown), but it did not reveal any significant activity against any kinase known to be involved in cell cycle regulation. We are in the process of investigating further the mechanism by which E235 induces senescence.

In summary, our results show that E235 induces ATF4 expression and establish a link between increased expression of ATF4 and the induction of DNA damage signaling. Further studies will need to be conducted to elucidate the mechanism by which E235 stimulates ATF4 expression and to determine the connection between ATF4 upregulation and the induction DNA damage signaling. Also, based on these promising *in vitro* results, we plan to begin studies in mice. The maximum tolerated dose of E235 and the effects of E235 on the growth of subcutaneous tumors will be examined.

Acknowledgments. We wish to thank George Cerniglia for his technical expertise and Stacey Lehman for generously providing the adult lung fibroblasts.

Authorship Contributions

Participated in research design: Sayers, Papandreou, Koong, Koumenis.

Conducted experiments: Sayers, Papandreou, Guttmann, Witze.

Contributed new reagents or analytic tools: Maas, Diehl.

Performed data analysis: Sayers, Papandreou, Guttmann, Koong.

Wrote or contributed to the writing of the manuscript: Sayers, Guttmann, Koumenis.

References

Ameri K, Lewis CE, Raida M, Sowter H, Hai T, Harris AL (2004) Anoxic induction of ATF-4 through HIF-1-independent pathways of protein stabilization in human cancer cells. *Blood* **103:** 1876-1882

Bartkova J, Horejsi Z, Koed K, Kramer A, Tort F, Zieger K, Guldberg P, Sehested M, Nesland JM, Lukas C, Orntoft T, Lukas J, Bartek J (2005) DNA damage response as a candidate anti-cancer barrier in early human tumorigenesis. *Nature* **434:** 864-870

Ben-Porath I, Weinberg RA (2005) The signals and pathways activating cellular senescence. *Int J Biochem Cell Biol* **37:** 961-976

Bi M, Naczki C, Koritzinsky M, Fels D, Blais J, Hu N, Harding H, Novoa I, Varia M, Raleigh J, Scheuner D, Kaufman RJ, Bell J, Ron D, Wouters BG, Koumenis C (2005) ER stress-regulated translation increases tolerance to extreme hypoxia and promotes tumor growth. *EMBO J* **24:** 3470-3481

Blais JD, Filipenko V, Bi M, Harding HP, Ron D, Koumenis C, Wouters BG, Bell JC (2004) Activating Transcription Factor 4 Is Translationally Regulated by Hypoxic Stress. *Mol Cell Biol* **24:** 7469-7482

Braig M, Lee S, Loddenkemper C, Rudolph C, Peters AHFM, Schlegelberger B, Stein H, Dorken B, Jenuwein T, Schmitt CA (2005) Oncogene-induced senescence as an initial barrier in lymphoma development. *Nature* **436:** 660-665

Brewer JW, Diehl JA (2000) PERK mediates cell-cycle exit during the mammalian unfolded protein response. *Proc Natl Acad Sci USA* **97:** 12625-12630

Chang B, Xuan Y, Broude E, Zhu H, Schott B, Fang J, Roninson I (1999) Role of p53 and p21waf1/cip1 in senescence-like terminal proliferation arrest induced in human tumor cells by chemotherapeutic drugs. *Oncogene* **18:** 4808-4818

Chao C, Saito Si, Anderson CW, Appella E, Xu Y (2000) Phosphorylation of murine p53 at Ser-18 regulates the p53 responses to DNA damage. *Proc Natl Acad Sci USA* **97:** 11936-11941

Chen J-J (2000) Heme-regulated eIF-2alpha kinase. In *Translational Control of Gene Expression*, Sonenberg N, Hershey J, Mathews M (eds), pp 529–546. Cold Spring Harbor, NY: Cold Spring Harbor Laboratory Press

Chen Z, Trotman LC, Shaffer D, Lin H-K, Dotan ZA, Niki M, Koutcher JA, Scher HI, Ludwig T, Gerald W, Cordon-Cardo C, Paolo Pandolfi P (2005) Crucial role of p53-dependent cellular senescence in suppression of Pten-deficient tumorigenesis. *Nature* **436:** 725-730

Collado M, Gil J, Efeyan A, Guerra C, Schuhmacher AJ, Barradas M, Benguria A, Zaballos A, Flores JM, Barbacid M, Beach D, Serrano M (2005) Tumour biology: Senescence in premalignant tumours. *Nature* **436:** 642-642

Coppé J-P, Kauser K, Campisi J, Beauséjour CM (2006) Secretion of Vascular Endothelial Growth Factor by Primary Human Fibroblasts at Senescence. *J Biol Chem* **281:** 29568-29574

Coppé J-P, Patil CK, Rodier F, Krtolica A, Beauséjour CM, Parrinello S, Hodgson JG, Chin K, Desprez P-Y, Campisi J (2010) A Human-Like Senescence-Associated Secretory Phenotype Is Conserved in Mouse Cells Dependent on Physiological Oxygen. *PLoS ONE* **5:** e9188

Coppé J-P, Patil CK, Rodier F, Sun Y, Muñoz DP, Goldstein J, Nelson PS, Desprez P-Y, Campisi J (2008) Senescence-Associated Secretory Phenotypes Reveal Cell-Nonautonomous Functions of Oncogenic RAS and the p53 Tumor Suppressor. *PLoS Biol* **6:** e301

Ewald JA, Desotelle JA, Wilding G, Jarrard DF (2010) Therapy-Induced Senescence in Cancer. *J Natl Cancer Inst* **102:** 1536-1546

Fels DR, Ye J, Segan AT, Kridel SJ, Spiotto M, Olson M, Koong AC, Koumenis C (2008) Preferential Cytotoxicity of Bortezomib toward Hypoxic Tumor Cells via Overactivation of Endoplasmic Reticulum Stress Pathways. *Cancer Res* **68:** 9323-9330

Friedman AD (1996) GADD153/CHOP, a DNA Damage-inducible Protein, Reduced CAAT/Enhancer Binding Protein Activities and Increased Apoptosis in 32D cl3 Myeloid Cells. *Cancer Res* **56:** 3250-3256

Hanahan D, Weinberg RA (2000) The Hallmarks of Cancer. *Cell* **100:** 57-70

Harding HP, Novoa I, Zhang Y, Zeng H, Wek R, Schapira M, Ron D (2000a) Regulated Translation Initiation Controls Stress-Induced Gene Expression in Mammalian Cells. *Mol Cell* **6:** 1099-1108

Harding HP, Zhang Y, Bertolotti A, Zeng H, Ron D (2000b) Perk Is Essential for Translational Regulation and Cell Survival during the Unfolded Protein Response. *Mol Cell* **5:** 897-904

Harding HP, Zhang Y, Zeng H, Novoa I, Lu PD, Calfon M, Sadri N, Yun C, Popko B, Paules R, Stojdl DF, Bell JC, Hettmann T, Leiden JM, Ron D (2003) An Integrated Stress Response Regulates Amino Acid Metabolism and Resistance to Oxidative Stress. *Mol Cell* **11:** 619-633

Kang MK, Kameta A, Shin K-H, Baluda MA, Kim H-R, Park N-H (2003) Senescence-associated genes in normal human oral keratinocytes. *Exp Cell Res* **287:** 272-281

Kaufman RJ (2002) Orchestrating the unfolded protein response in health and disease. *J Clin Invest* **110:** 1389-1398

Koumenis C (2006) ER stress, hypoxia tolerance and tumor progression. *Curr Mol Med* **6:** 55-69

Koumenis C, Naczki C, Koritzinsky M, Rastani S, Diehl A, Sonenberg N, Koromilas A, Wouters BG (2002) Regulation of Protein Synthesis by Hypoxia via Activation of the Endoplasmic Reticulum Kinase PERK and Phosphorylation of the Translation Initiation Factor eIF2alpha. *Mol Cell Biol* **22:** 7405-7416

Krtolica A, Parrinello S, Lockett S, Desprez P-Y, Campisi J (2001) Senescent fibroblasts promote epithelial cell growth and tumorigenesis: A link between cancer and aging. *Proc Natl Acad Sci USA* **98:** 12072-12077

Ksiazek K, Jörres A, Witowski J (2008) Senescence induces a proangiogenic switch in human peritoneal mesothelial cells. *Rejuvenation Res* **11:** 681-683

Lee AS (1992) Mammalian stress response: induction of the glucose-regulated protein family. *Curr Opin Cell Biol* **4:** 267-273

Levin D, Petryshyn R, London I (1980) Characterization of double-stranded-RNA-activated kinase that phosphorylates alpha subunit of eukaryotic initiation factor 2 (eIF-2 alpha) in reticulocyte lysates. *Proc Natl Acad Sci USA* **77:** 832-836

Levine AJ (1997) p53, the Cellular Gatekeeper for Growth and Division. *Cell* **88:** 323-331

Michaloglou C, Vredeveld LCW, Soengas MS, Denoyelle C, Kuilman T, van der Horst CMAM, Majoor DM, Shay JW, Mooi WJ, Peeper DS (2005) BRAFE600-associated senescence-like cell cycle arrest of human naevi. *Nature* **436:** 720-724

Millis A, Hoyle M, McCue H, Martini H (1992) Differential expression of metalloproteinase and tissue inhibitor of metalloproteinase genes in aged human fibroblasts. *Exp Cell Res* **201:** 373-379

Obeng EA, Carlson LM, Gutman DM, Harrington WJ, Lee KP, Boise LH (2006) Proteasome inhibitors induce a terminal unfolded protein response in multiple myeloma cells. *Blood* **107:** 4907-4916

Rodier F, Campisi J (2011) Four faces of cellular senescence. *J Cell Biol* **192:** 547-556

Scheuner D, Song B, McEwen E, Liu C, Laybutt R, Gillespie P, Saunders T, Bonner-Weir S, Kaufman RJ (2001) Translational Control Is Required for the Unfolded Protein Response and In Vivo Glucose Homeostasis. *Mol Cell* **7:** 1165-1176

Shi Y, Vattem KM, Sood R, An J, Liang J, Stramm L, Wek RC (1998) Identification and Characterization of Pancreatic Eukaryotic Initiation Factor 2 α-Subunit Kinase, PEK, Involved in Translational Control. *Mol Cell Biol* **18:** 7499-7509

Vattem KM, Wek RC (2004) Reinitiation involving upstream ORFs regulates ATF4 mRNA translation in mammalian cells. *Proc Natl Acad Sci USA* **101:** 11269-11274

Wek SA, Zhu S, Wek RC (1995) The histidyl-tRNA synthetase-related sequence in the eIF-2 alpha protein kinase GCN2 interacts with tRNA and is required for activation in response to starvation for different amino acids. *Mol Cell Biol* **15:** 4497-4506

Ye J, Kumanova M, Hart LS, Sloane K, Zhang H, De Panis DN, Bobrovnikova-Marjon E, Diehl JA, Ron D, Koumenis C (2010) The GCN2-ATF4 pathway is critical for tumour cell survival and proliferation in response to nutrient deprivation. *EMBO J* **29:** 2082-2096

Zinszner H, Kuroda M, Wang X, Batchvarova N, Lightfoot RT, Remotti H, Stevens JL, Ron D (1998) CHOP is implicated in programmed cell death in response to impaired function of the endoplasmic□reticulum. *Genes Dev* **12:** 982-995

Footnotes

This work was supported by the National Institutes of Health National Cancer Institute [Grant 5-R01-CA-139362-04]. C.M.S. was supported by the National Institutes of Health National Cancer Institute Fellowship Training [Grant 5-T32-CA-009677-20].

Current address (Ioanna Papandreou): Department of Radiation Oncology, Ohio State University School of Medicine, Columbus, Ohio 43210.

This work was previously presented at two conferences:

Lehman SL, Sayers CM, Ye J, Hart LS, Ayeni DO, Koong AC, and Koumenis C. The Role of the Integrated Stress Response Proteins GCN2 and ATF4 in Autophagy and Tumor Migration [abstract]. In: Proceedings of the 102nd Annual Meeting of the American Association for Cancer Research; 2011 Apr 2-6; Orlando, FL. Philadelphia (PA): AACR; 2011.

Sayers CM, Guttmann DG, Koong AC, Koumenis C. An Integrated Stress Response Activator Causes Cellular Senescence and Inhibits Growth in Multiple Tumor Cell Types [abstract]. In: Proceedings of the 103rd Annual Meeting of the American Association for Cancer Research; 2012 Mar 31 – Apr 4; Chicago, IL. Philadelphia (PA): AACR; 2012.

For reprints:

Constantinos Koumenis

Address: Department of Radiation Oncology, Univ. of Pennsylvania Perelman School of Medicine, Translational Research Center Room 8th Floor, 3400 Civic Center Blvd., Bldg 421, Philadelphia, PA 19104-5156

Email: costas.koumenis@uphs.upenn.edu

Molecular Pharmacology Fast Forward. Published on December 10, 2012 as DOI: 10.1124/mol.112.081810
This article has not been copyedited and formatted. The final version may differ from this version.

Figure Legends

Fig. 1. Treatment with E235 increases ATF4 expression. A, Schematic of the ATF4-luciferase reporter construct used in the chemical library screen. B, Chemical structure of E235. C, Induction of ATF4 translation was analyzed by measuring luciferase activity in HT1080 cells transfected with ATF4-Luc. Luciferase activity was measured at 0, 4, and 8 hours after treatment with 1 or 10μM E235. Fold change was determined by dividing the ATF4-Luc signal by the signal from a constitutively active reporter plasmid (CMV-Luc). *p<0.05 or ***p<0.001 as compared to DMSO-treated controls (student's t-test; n=3). D-F, ATF4 protein expression in HT1080 (D), B16F10 (E), and AG1522 (F) cells was examined by immunoblotting after 4 hours of treatment with 0, 1, 5, or 10μM E235. Thapsigargin treatment (0.5μM for 4h) was included as a positive control. Ku80 was used as a loading control.

Fig. 2. E235 induces the ISR in transformed cells. A-B, HT1080 cells were treated with either 1μM E235 for various times (A) or with increasing doses of E235 for 4h (B) and activation of the ISR was examined by blotting whole cell lysates for phosphorylated eIF2α (p-eIF2α) and PERK. Lysate from HT1080 cells treated with 0.5μM Tg for 1h was used as a positive control. Ku80 was used as a loading control. C, AG1522 cells were treated with increases doses of E235 and levels of p-eIF2α were determined by immunoblotting. Ku80 was used as a loading control. D, Quantitative PCR was used to determine the levels of XBP1-s mRNA in HT1080 cells after various lengths of 1μM E235 treatment. Treatment with 0.5μM Tg for 4h was used as a positive control. All XBP1-s values were normalized to 18s rRNA levels and then to the DMSO-treated control (0μM) value. **p<0.01 as compared to control (0μM) by student's t-test (one sample read in triplicate). E, Activation of the ISR in empty vector and shPERK transduced HT1080 cells

Molecular Pharmacology Fast Forward. Published on December 10, 2012 as DOI: 10.1124/mol.112.081810
This article has not been copyedited and formatted. The final version may differ from this version.

treated with E235 was examined by immunoblotting whole cell lysates for p-eIF2α and PERK. Cells treated for 1h with 0.5μM Tg were used as a positive control. Ku80 was used as a loading control.

Fig. 3. E235 decreases cell proliferation. A, Various cell lines were treated with increasing doses of E235 and effects on cell proliferation were assessed using an MTT assay. E235 treatment was for either 4 days (4T1 and B16F10) or 5 days (HT1080 and RPMI-8226). The cell lines tested were HT1080, RPMI-8226, B16F10, and 4T1. All E235 treatment groups were normalized to DMSO-treated (0μM) controls. **p<0.01, ***p<0.001 as compared to 0μM controls. B, HT1080 or RPMI-8226 cells were treated with 1μM E235 for the indicated time periods. At those times, fresh media without E235 was added and cells were allowed to proliferate until the untreated cells reached confluency (5 days after initial treatment). Cell proliferation/survival was then measured with an MTT assay. C, Cell viability was examined in normal human fibroblasts using the MTT assay. AG1522 cells were treated with various doses of E235 for 4 days. All E235 treatment groups were normalized to untreated controls. ***p<0.001 as compared to untreated controls. Data (A-C) presented as the mean ± SEM (n=6), and all statistics were performed using one-way ANOVA with Tukey's multiple comparison post-test. D-E, Expression of the apoptotic markers c-PARP and cleaved caspase3 (c-casp3), after varying lengths and doses of E235 treatment, was examined by immunoblotting in both HT1080 (D) and B16F10 (E) cells. Treatments with 1μM Tg (4h) or 0.5μM staurosporine (Stauro) (3h) were used as positive controls. Ku80 was used as a loading control.

Fig. 4. Ablation of ATF4 enhances E235-induced decrease in cell viability. A, Western of nuclear lysates from HT1080 shNT and shATF4 cells treated with DMSO or Tg (4h) showing the

efficiency of ATF4 knockdown. Ku80 was used as a loading control. B, The importance of ATF4 for the E235-induced reduction in cell viability was assessed with an MTT assay using HT1080 shNT or shATF4 cells. Cells were treated with various doses of E235 for 5 days. All E235 treatment groups were normalized to DMSO-treated (0μM) controls. **p<0.01 or ***p<0.001 as compared to 0μM controls using one-way ANOVA with Tukey's multiple comparison post-test. C, The influence of ATF4 expression on the viability of cells treated with E235 was also analyzed with a clonogenic assay. Surviving fraction of each cell type is plotted vs. the log of the E235 concentration. Each data point is n=3. ***p=0.0003 for shNT vs. shATF4 at 1μM E235 by student's t-test.

Fig. 5. E235 induces upregulation of p21 and a senescence-like phenotype at low doses. A, Phase microscopy images of B16F10 and mouse ALF cells after 3 and 5 days, respectively, of DMSO or E235 treatment. Original objective magnification was 10x. B-C, HT1080 (B) and B16F10 (C) cells were treated for various lengths and doses of E235, and expression of the senescence regulators p21 and p27 were analyzed by immunoblotting. Ku80 expression was used as a loading control. D, B16F10 cells stably transfected with either pLKO or shP21 (two different clones) were treated with E235 for 48h and then stained for SA-β-gal activity. Original objective magnification was 10x. E, The effect of knocking down p21 expression on cell viability was examined using an MTT assay. B16F10 pLKO or shP21 cells were treated with various doses of E235 for 4 days. All treatment groups were normalized to their respective DMSO-treated (0μM) controls. ****p<0.0001 for each shP21 clone as compared to pLKO cells treated with the same dose. Representative data from one of two separate experiments is shown and is presented as the mean ± SEM (n=6). Statistics were performed using one-way ANOVA with Tukey's multiple comparison post-test.

Molecular Pharmacology Fast Forward. Published on December 10, 2012 as DOI: 10.1124/mol.112.081810
This article has not been copyedited and formatted. The final version may differ from this version.

Fig. 6. E235 causes cell cycle arrest at G2/M. A-B, HT1080 (A) and B16F10 (B) cells were treated with 1μM E235 for various lengths of time and then stained with PI. PI-stained cells were analyzed for cell cycle distribution using flow cytometry. Each graph depicts fluorescent intensity vs. cell count of about 20,000 total events. The percentages of cells in G1, S, and G2 phases are listed within each graph.

Fig.7. E235 promotes DNA damage signaling but does not induce DNA double strand breaks. A-B, AG1522 and HT1080 cells were treated with increasing doses of E235 (for 4h), and the stabilization of p53 was determined by immunoblotting whole cell lysates for total p53 (A). In addition, the induction of p53 phosphorylation was assessed by blotting with an antibody specific for phosphorylation of p53 on Ser15 (B). As a positive control, AG1522 cells were irradiated with 4Gy and harvested 2h later. C, Both AG1522 and HT1080 cells were treated with various doses of E235 and γ-H2AX levels were determined by immunoblotting. Cells treated with 4Gy of radiation and harvested 30 min later were used as a positive control. D, Unsynchronized and synchronized (with 400ng/ml of nocodazole (Noc) for 16h) HT1080 cells were analyzed for p-Chk2 (Thr68) levels after 2h of treatment with either DMSO or 1μM E235. E, HT1080 shNT and shATF4 cells were treated with increasing doses of E235, and the levels of γ-H2AX were analyzed by immunoblotting. Values below the blots represent fold change in γ-H2AX pixel intensity over DMSO-treated shNT cells after normalization to Ku80 levels. Cells irradiated with 4Gy (harvested after 15min) were used as a positive control. The immunoblots shown are representative of 3 independent experiments. Ku80 was used as a loading control for A-E. F-G, A comet assay was performed on E235-treated AG1522 and HT1080 cells to assess DNA double strand breaks. Cells were treated with E235 for 24h. Tail moments of individual cells were quantified and the median tail moment is presented in the graph (G). Cells irradiated

Molecular Pharmacology Fast Forward. Published on December 10, 2012 as DOI: 10.1124/mol.112.081810
This article has not been copyedited and formatted. The final version may differ from this version.

with 4Gy (assayed immediately) were used as a positive control. Representative images of the treatment groups in HT1080 cells are shown (F).

Figure 1

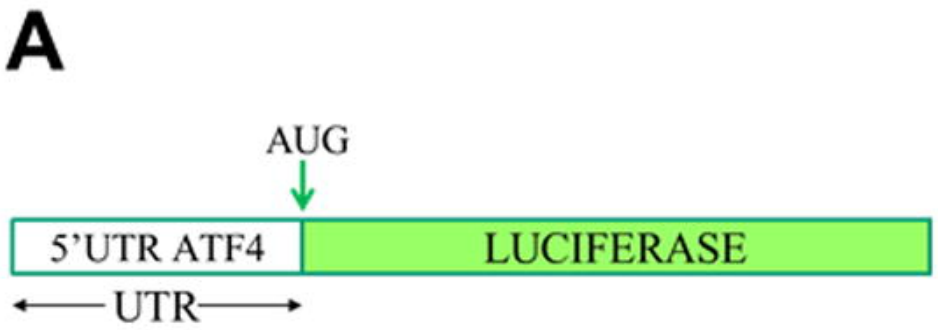
A
AUG
5'UTR ATF4
LUCIFERASE
UTR

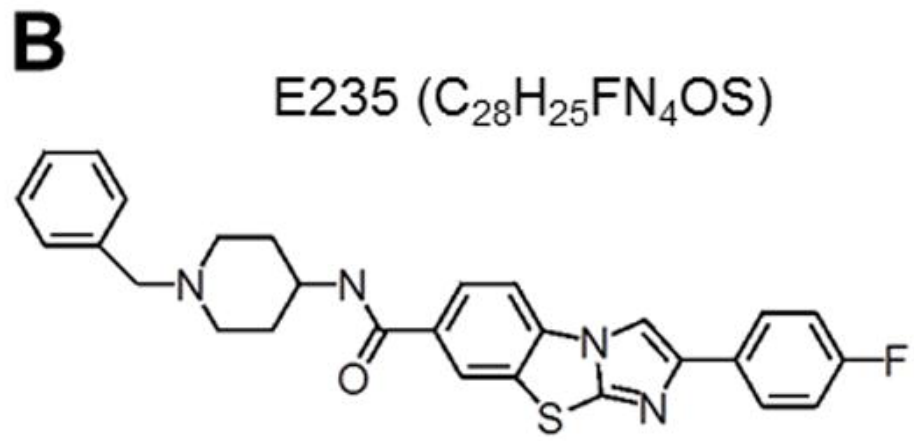
B
E235 ($C_{28}H_{25}FN_4OS$)
N
N
O
N
S
N
F

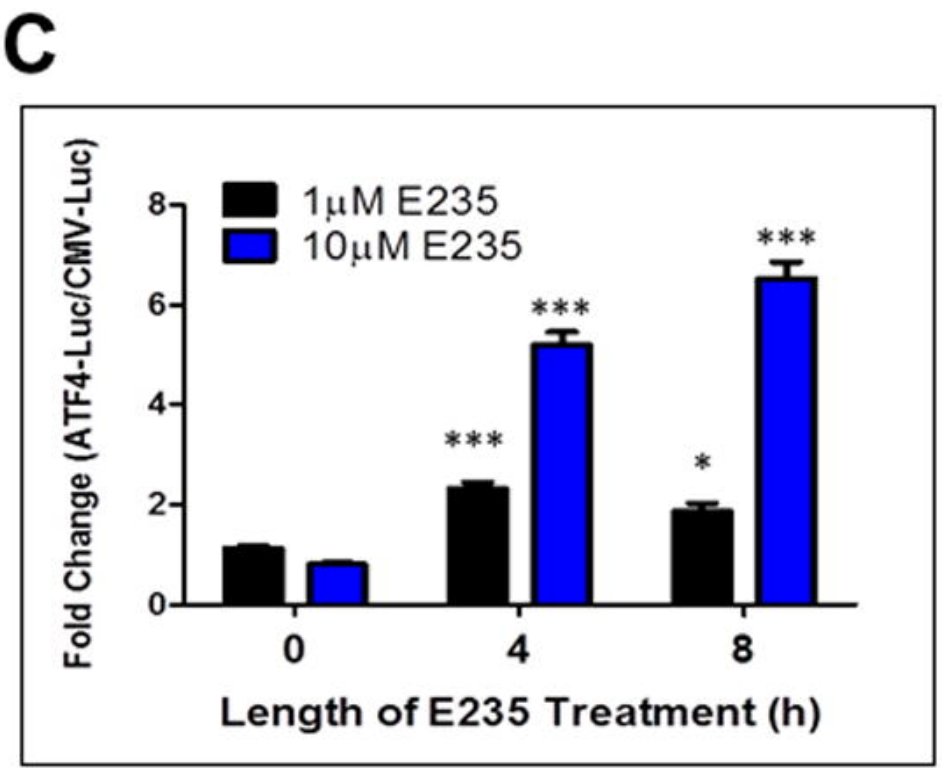
C
Fold Change (ATF4-Luc/CMV-Luc)
1μM E235
10μM E235
***
***
***
*
0
2
4
6
8
0
4
8
Length of E235 Treatment (h)

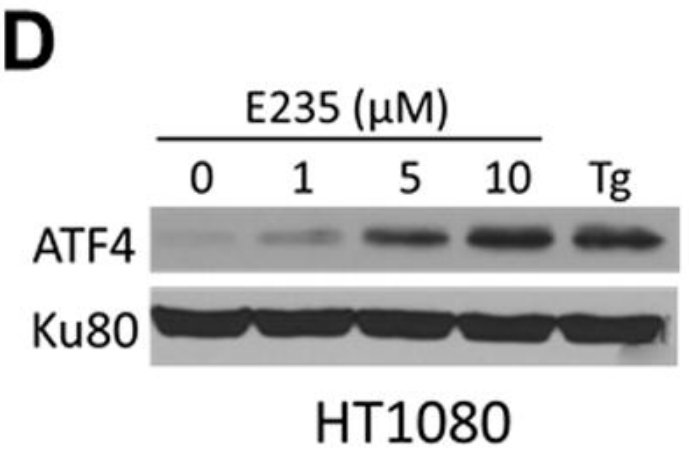
D
E235 (μM)
0
1
5
10
Tg
ATF4
Ku80
HT1080

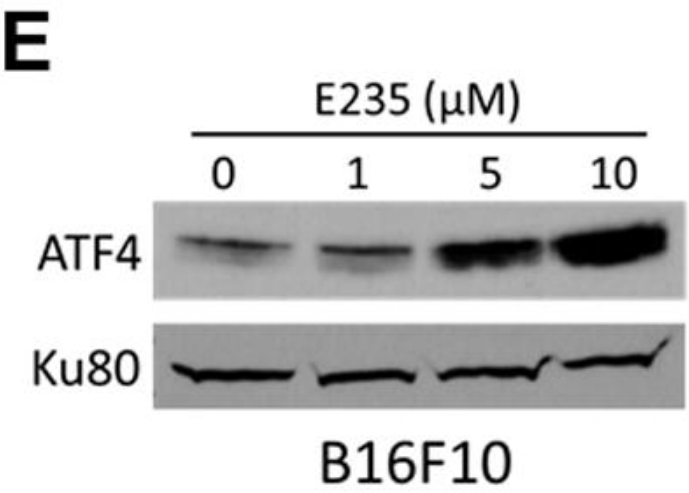
E
E235 (μM)
0
1
5
10
ATF4
Ku80
B16F10

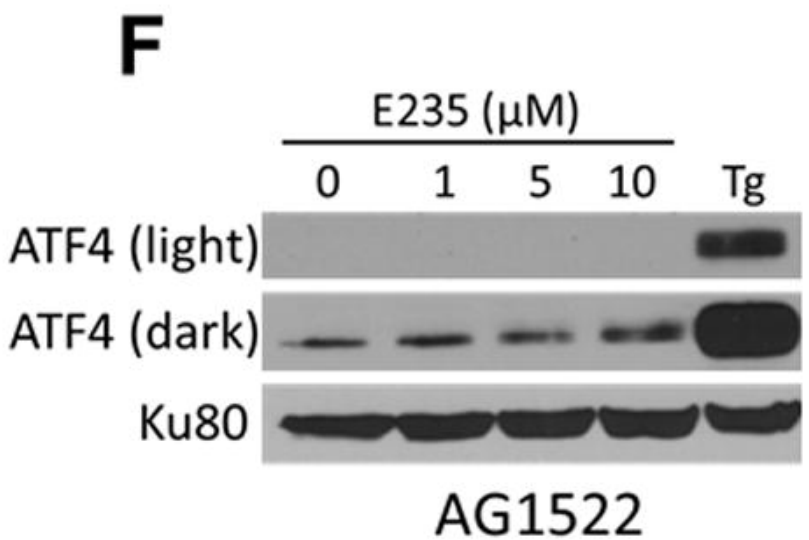
F
E235 (μM)
0
1
5
10
Tg
ATF4 (light)
ATF4 (dark)
Ku80
AG1522

Figure 2

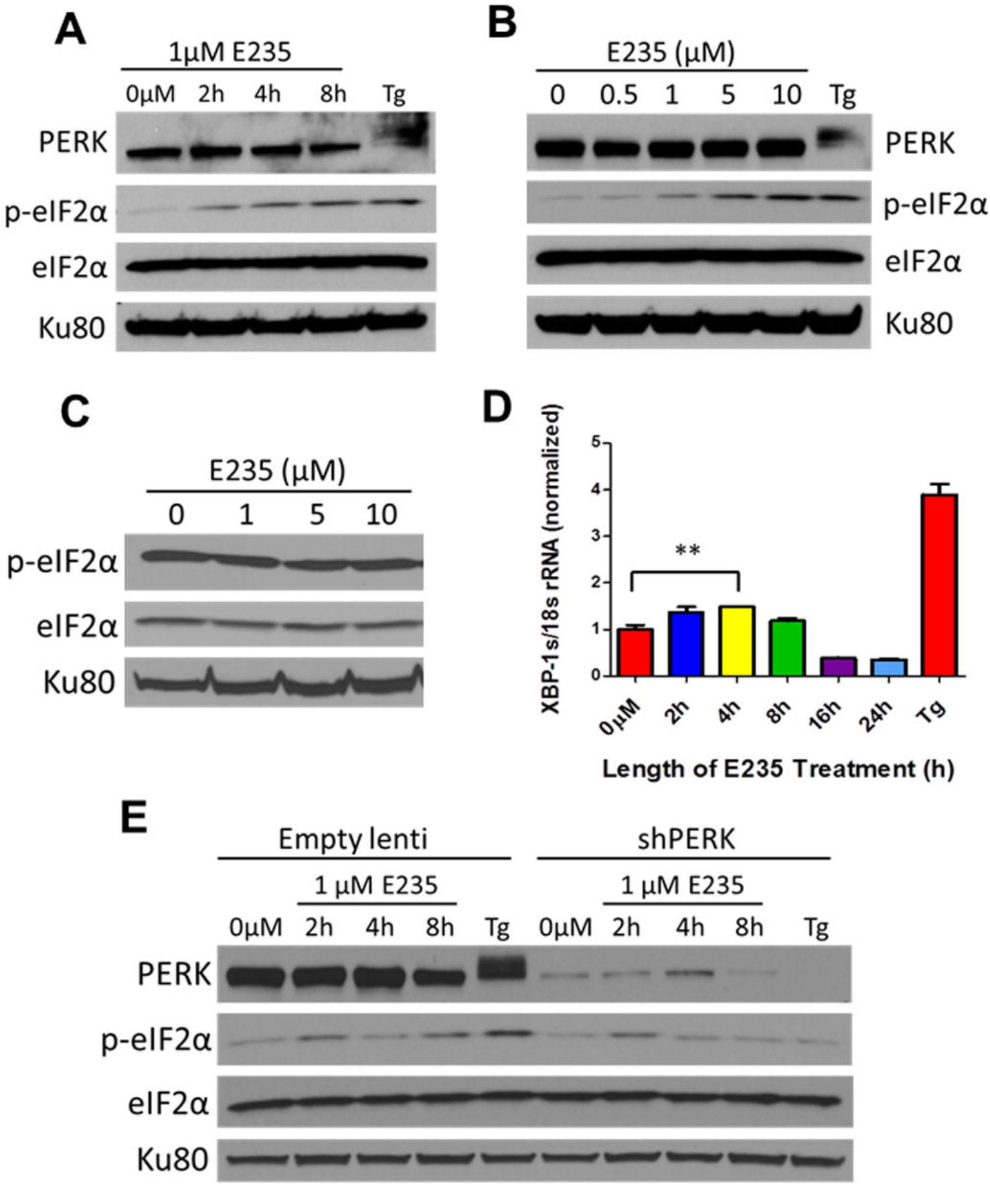
A
1μM E235
0μM 2h 4h 8h Tg
PERK
p-eIF2α
eIF2α
Ku80
B
E235 (μM)
0 0.5 1 5 10 Tg
PERK
p-eIF2α
eIF2α
Ku80
C
E235 (μM)
0 1 5 10
p-eIF2α
eIF2α
Ku80
D
XBP-1s/18s rRNA (normalized)
**
0μM 2h 4h 8h 16h 24h Tg
Length of E235 Treatment (h)
E
Empty lenti
shPERK
1 μM E235
1 μM E235
0μM 2h 4h 8h Tg 0μM 2h 4h 8h Tg
PERK
p-eIF2α
eIF2α
Ku80

Figure 3

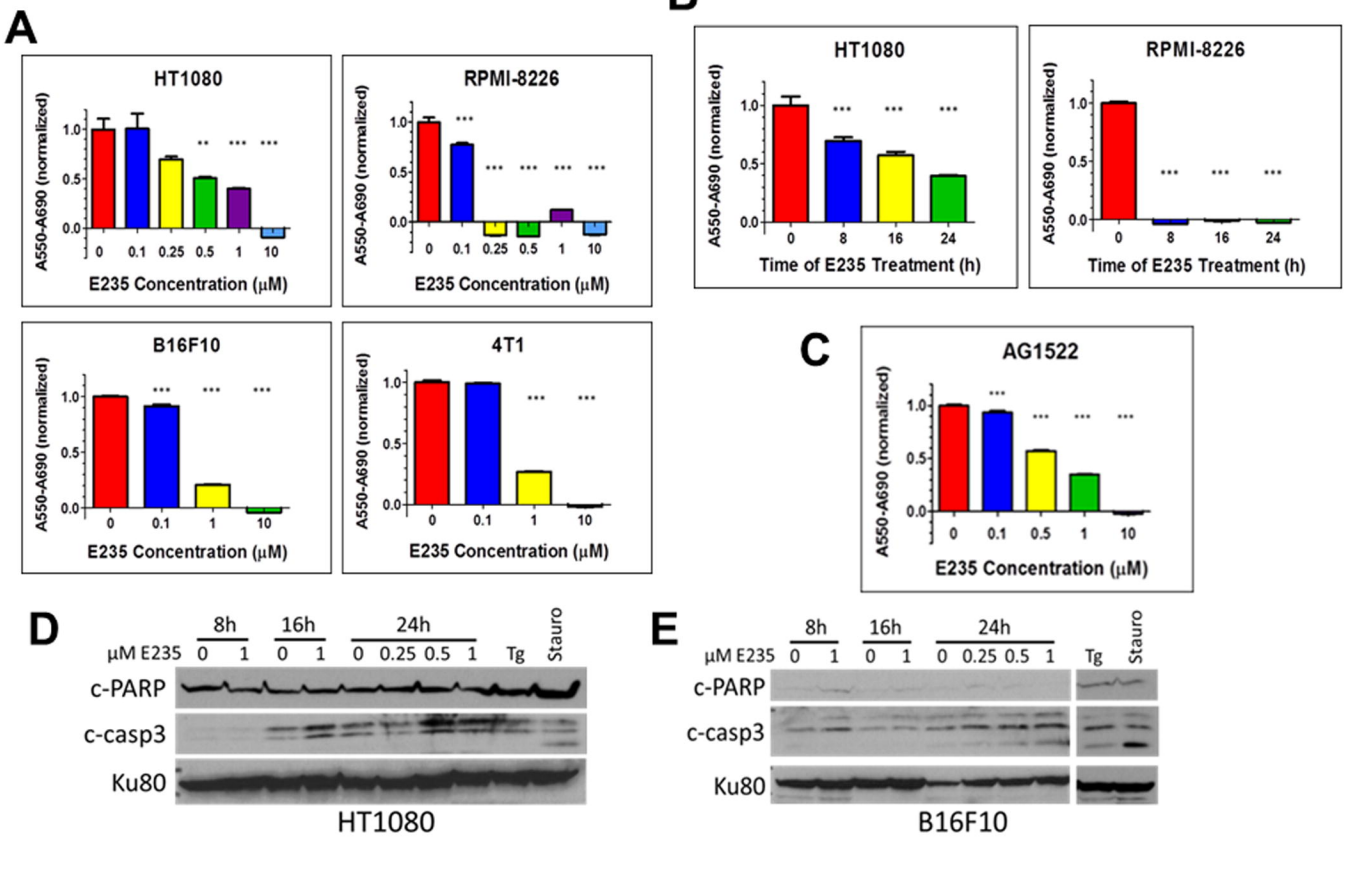
A
HT1080
RPMI-8226
B16F10
4T1
A550-A690 (normalized)
E235 Concentration (μM)
B
HT1080
RPMI-8226
Time of E235 Treatment (h)
C
AG1522
D
8h
16h
24h
μM E235
Tg
Stauro
c-PARP
c-casp3
Ku80
HT1080
E
B16F10

Figure 4

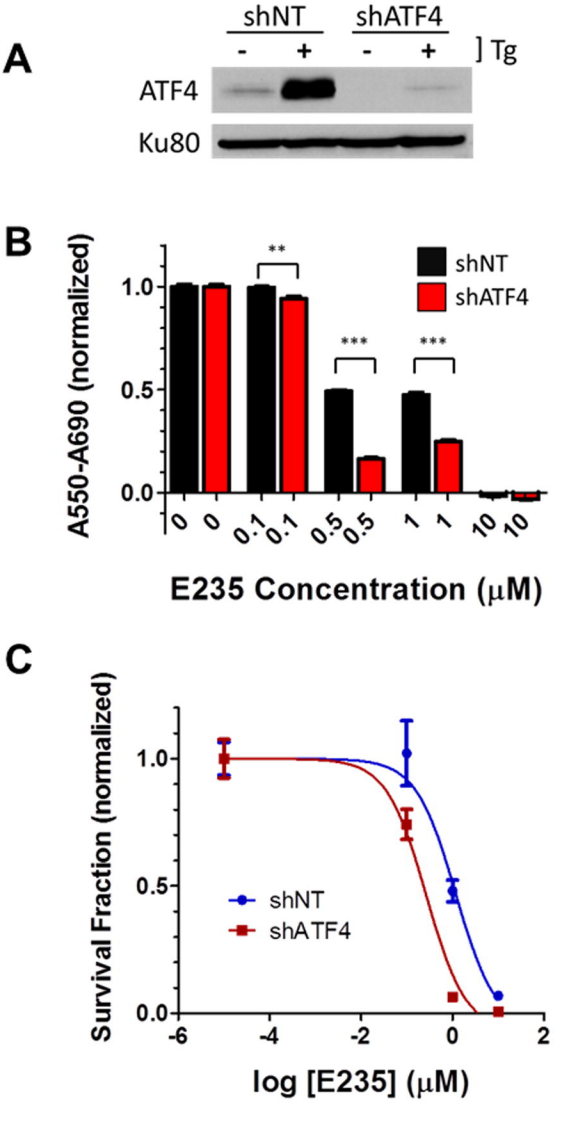
A
shNT
shATF4
- + - +] Tg
ATF4
Ku80
B
A550-A690 (normalized)
shNT
shATF4
**
***
***
1.0
0.5
0.0
0 0 0.1 0.1 0.5 0.5 1 1 10 10
E235 Concentration (μM)
C
Survival Fraction (normalized)
1.0
0.5
0.0
shNT
shATF4
-6 -4 -2 0 2
log [E235] (μM)

Figure 5

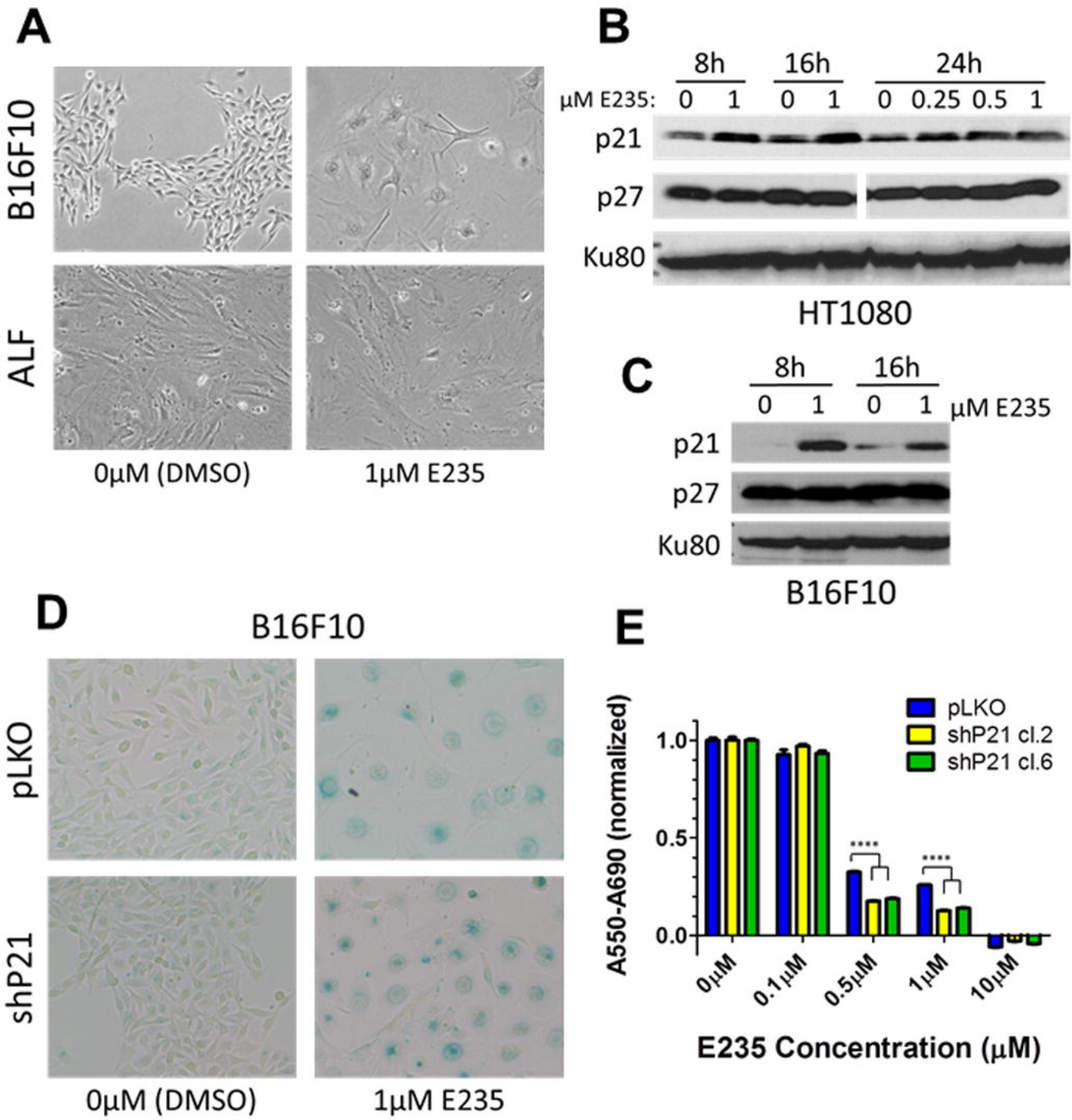
A
B16F10
ALF
0μM (DMSO)
1μM E235
B
8h
16h
24h
μM E235: 0 1 0 1 0 0.25 0.5 1
p21
p27
Ku80
HT1080
C
8h
16h
0 1 0 1 μM E235
p21
p27
Ku80
B16F10
D
B16F10
pLKO
shP21
0μM (DMSO)
1μM E235
E
pLKO
shP21 cl.2
shP21 cl.6
A550-A690 (normalized)
1.0
0.5
0.0
****
****
0μM
0.1μM
0.5μM
1μM
10μM
E235 Concentration (μM)

Figure 6

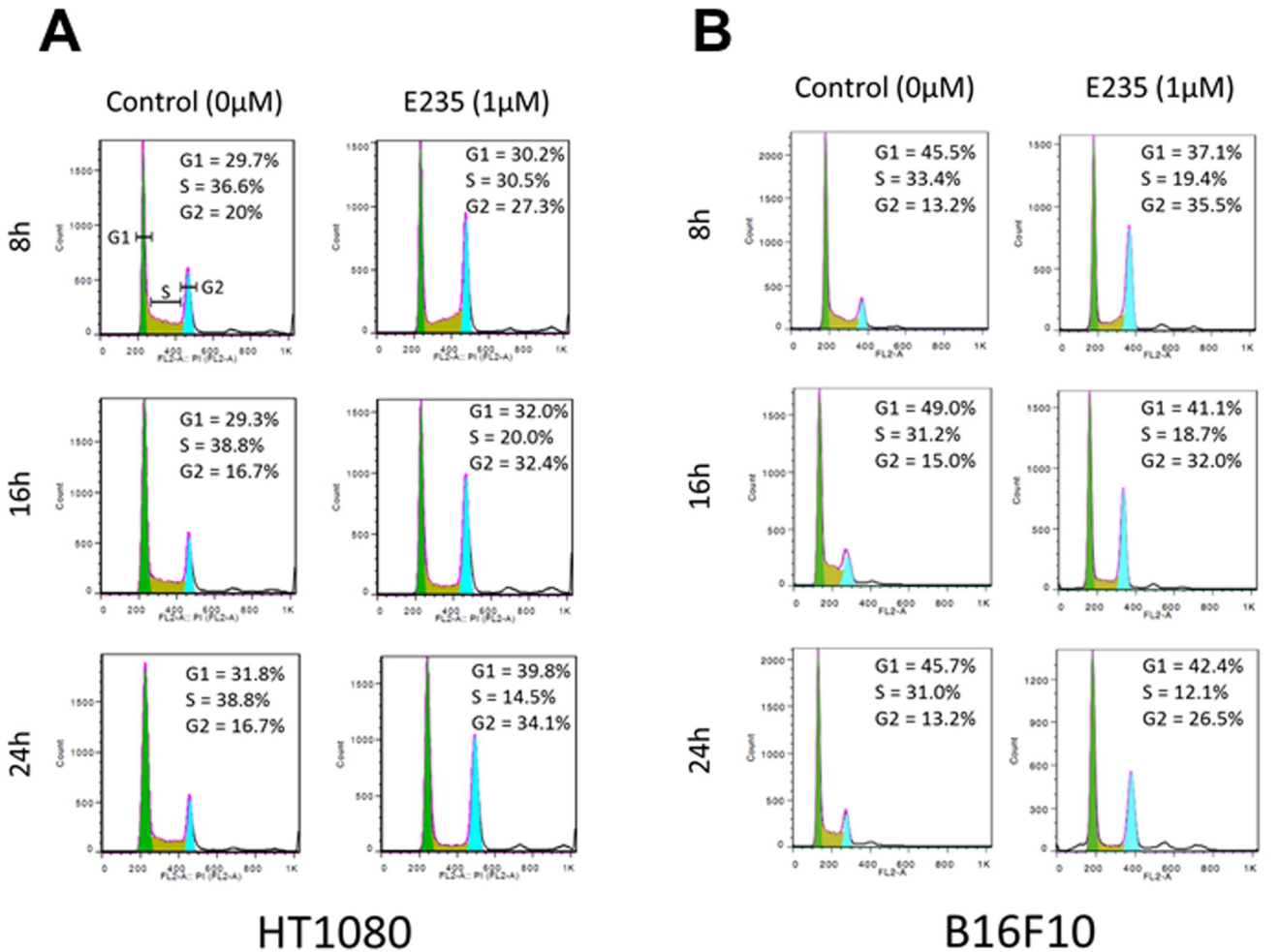
A
Control (0μM)
E235 (1μM)
8h
16h
24h
G1 = 29.7%
S = 36.6%
G2 = 20%
G1 = 30.2%
S = 30.5%
G2 = 27.3%
G1 = 29.3%
S = 38.8%
G2 = 16.7%
G1 = 32.0%
S = 20.0%
G2 = 32.4%
G1 = 31.8%
S = 38.8%
G2 = 16.7%
G1 = 39.8%
S = 14.5%
G2 = 34.1%
HT1080
B
Control (0μM)
E235 (1μM)
8h
16h
24h
G1 = 45.5%
S = 33.4%
G2 = 13.2%
G1 = 37.1%
S = 19.4%
G2 = 35.5%
G1 = 49.0%
S = 31.2%
G2 = 15.0%
G1 = 41.1%
S = 18.7%
G2 = 32.0%
G1 = 45.7%
S = 31.0%
G2 = 13.2%
G1 = 42.4%
S = 12.1%
G2 = 26.5%
B16F10

Figure 7

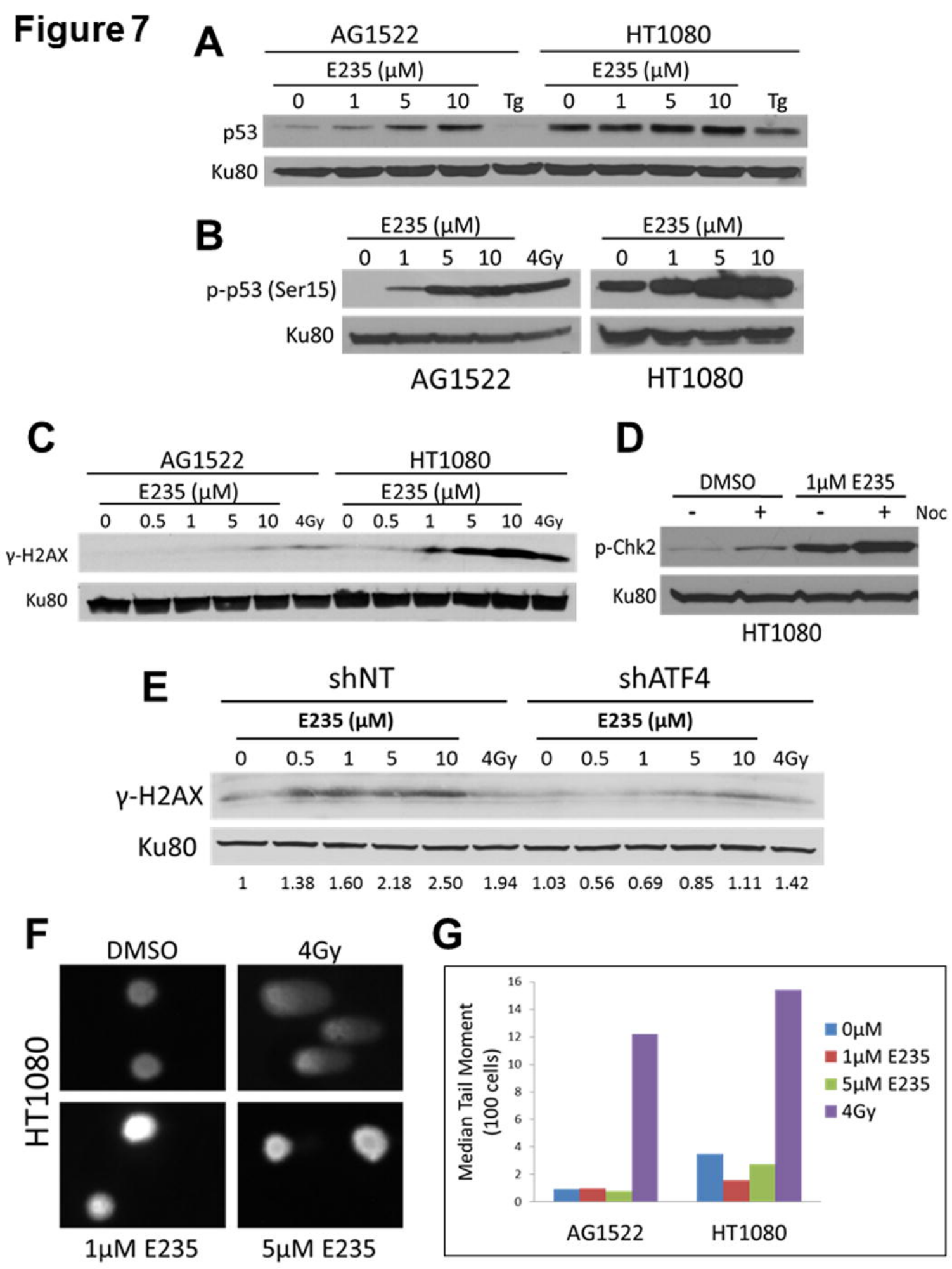
A
AG1522
HT1080
E235 (μM)
E235 (μM)
0 1 5 10 Tg 0 1 5 10 Tg
p53
Ku80
B
E235 (μM)
E235 (μM)
0 1 5 10 4Gy 0 1 5 10
p-p53 (Ser15)
Ku80
AG1522
HT1080
C
AG1522
HT1080
E235 (μM)
E235 (μM)
0 0.5 1 5 10 4Gy 0 0.5 1 5 10 4Gy
γ-H2AX
Ku80
D
DMSO
1μM E235
- + - + Noc
p-Chk2
Ku80
HT1080
E
shNT
shATF4
E235 (μM)
E235 (μM)
0 0.5 1 5 10 4Gy 0 0.5 1 5 10 4Gy
γ-H2AX
Ku80
1 1.38 1.60 2.18 2.50 1.94 1.03 0.56 0.69 0.85 1.11 1.42
F
DMSO
4Gy
HT1080
1μM E235
5μM E235
G
Median Tail Moment (100 cells)
0 2 4 6 8 10 12 14 16
0μM
1μM E235
5μM E235
4Gy
AG1522
HT1080